AD-A163 025 MODIFICATION OF THE IONOSPHERIC ELECTRON VELOCITY DISTRIBUTION FUNCTION D (U) CALIFORNIA UNIV LOS ANGELES CENTER FOR PLASMA PHYSICS AND FUS 1/1

UNCLASSIFIED M SHOUCRI ET AL DEC 85 PPG-913 F/G 4/1 NL

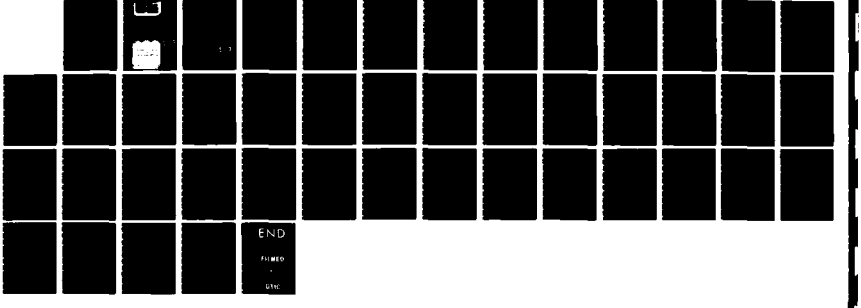

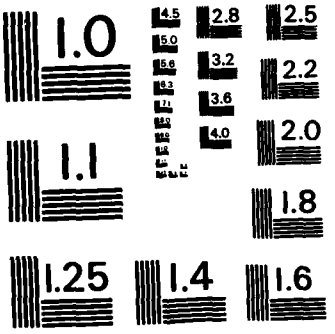

MODIFICATION OF THE IONOSPHERIC ELECTRON VELOCITY DISTRIBUTION FUNCTION DUE TO RESONANT ABSORPTION OF HF WAVES

Merit Shoucri, G.J. Morales, & J.E. Maggs

December 1985 PPG-913

CENTER FOR PLASMA PHYSICS AND FUSION ENGINEERING

UNIVERSITY OF CALIFORNIA LOS ANGELES

(3)

MODIFICATION OF THE IONOSPHERIC ELECTRON VELOCITY DISTRIBUTION FUNCTION DUE TO RESONANT ABSORPTION OF HF WAVES

Merit Shoucri, G.J. Morales, & J.E. Maggs

December 1985 PPG-913

Contract N00014-75-C-0476

University of California

Department of Physics

Los Angeles, CA 90024

MODIFICATION OF THE IONOSPHERIC ELECTRON VELOCITY DISTRIBUTION FUNCTION DUE TO RESONANT ABSORPTION OF HF WAVES

Merit Shoucri, G.J. Morales, and J.E. Maggs

Physics Department

University of California at Los Angeles

Los Angeles, CA 90024

ABSTRACT

The nonlinear modification of the electron distribution function caused by the interaction with a resonant electrostatic field is studied analytically using a perturbation analysis. This interaction produces tail heating, and for a range of parameter values, can form a bump in the distribution, which leads to emission of secondary waves. These results are applied to the ionosphere's F and upper E regions in the context of ionospheric modification experiments using ground-based powerful HF transmitters. Analogies between our results and experimental measurements are discussed.

1. INTRODUCTION

The interaction of powerful high frequency (HF) electromagnetic waves with ionospheric plasmas can lead to the generation of electrostatic plasma waves through various processes, e.g., linear mode conversion, direct conversion, parametric instabilities, etc. These processes occur at a height where the angular frequency of the HF wave ω_o nearly matches the local electron plasma frequency ω_p. The relatively slow phase velocity of the excited electrostatic modes allows the possibility of strong interactions with ionospheric electrons. These interactions can result in significant modifications of the background electron distribution function. The signatures of such interactions are often observed during ionospheric modification experiments [see, for reference, volume 9, issue 11, of Radio Science (1974), and volume 44, issue 12, of Journal of Atmospheric and Terrestrial Physics (1982)]. For example, during HF heating experiments, fast electrons produce enhanced airglow at 6300Å and 5577Å, caused by the excitation of atomic oxygen lines [Sipler and Biondi, 1972; Haslett and Megill, 1974; Carleson, et al., 1982]. Non-ohmic heating of the ionosphere which is partially attributed to tail particles produced during the HF heating has also been observed [Meltz, et al., 1974; Mantas, et al., 1981]. The purpose of the present work is to calculate the modification in the electron velocity distribution function resulting from the resonant excitation of electrostatic oscillations in the ionosphere. It is hoped that the analytic results may help illuminate some of the various experimentally observed phenomena, and perhaps suggest new experiments which would probe the nature of the electron acceleration mechanisms.

This study does not address the different mechanisms that can generate plasma waves. Such studies are available in the literature. For example, the generalized mode conversion problem is treated in detail by Mjølhus [1983]; direct conversion is analyzed by Wong, et al., [1981]; and parametric instabilities in the ionosphere are reviewed by Fejer [1979]. The present work assumes a given spatial structure for the electric field near the plasma resonance, and proceeds to calculate the resultant kinetic interactions. Two typical resonant structures are considered: one corresponds to the convective limitation of the plasma resonance (Airy pattern), and the other is appropriate to a collisionally limited resonance (Lorentzian pattern).

Figure 1 illustrates the geometry of the model problem, and shows the relevant scales. The localized electrostatic field $E_{\parallel}(z)$ is considered to be parallel to the earth's magnetic field $\vec{B}_o$ at $z = 0$. Its characteristic width is $\Delta z_i \sim L_n(k_D L_n)^{-2/3}$ for the Airy pattern, or $\Delta z_i \sim (\Gamma L_n)$ for the Lorentzian pattern, where $\Gamma = \nu_e/\omega_o$, ν_e is the electron collision frequency, L_n the density scalelength along $\vec{B}_o$, and k_D is the Debye wavenumber. Electrons impinging upon the localized field from the high density side can be accelerated as they pass through the interaction region Δz_i, hence, modifying the distribution function downstream at $z = z_o$. This modified distribution changes slowly within a slowing down length L(u) for those electrons with velocity u parallel to the magnetic field; beyond L(u), the distribution relaxes to an appropriate equilibrium.

In this work, we analytically calculate the modified electron distribution existing in the range between z_o and L(u) by using a perturbation analysis correct to second order in the strength of the electric field. The

general result we derive is applied to a specific bi-Maxwellian background electron distribution, characteristic of an ionospheric F region. Parameters of the background plasma are varied to assess the effect of different ionospheric conditions.

An interesting feature found in the analysis of the Airy and Lorentzian patterns is that both structures have a broadband, unidirectional Fourier spectrum, with identical power spectra characterized by a collisionally dependent exponential envelope. For electric field amplitudes above a certain threshold, a bump can be formed in the tail of the velocity distribution function downstream from the resonance layer. The region of positive slope in the velocity distribution may trigger the growth of a broad spectrum of sideband waves in the neighborhood of ω_0. The width of the sideband frequency spectrum is determined by the electric field strength, its effective phase velocity, and by the background plasma parameters. It is worth noting that these sidebands are analogous to ones observed in the laboratory by Starke and Malmberg [1978]. Another interesting result obtained from the calculation is the observation of heating of particles with velocities of the order of, or larger than, the characteristic phase velocity of the resonant field. These tail electrons ultimately loose their energy to neutral particles and bulk electrons by different collisional processes that occur in the ionosphere. The observed airglow enhancement is but one of these processes. Through them one can estimate the slowing down length for fast electrons.

The description and analysis of the model are presented in section 2. Results obtained from the model are discussed in section 3, while conclusions are given in section 4.

2. MODEL

This analysis considers a nonuniform, weakly collisional ($\nu_e << \omega_o$), magnetized plasma characteristic of the ionospheric F and upper E regions. The resonantly excited electric fields are assumed to be primarily aligned along the magnetic field $\hat{z}B_o$, i.e.,

$$\vec{E}(\vec{r},t) = \hat{z}\,[E_\parallel(z)\exp(-i\omega_o t) + c.c.]\ ; \tag{1}$$

hence, the Boltzmann equation is solved by separating the total distribution function $f(\vec{r},\vec{v},t)$ into an unperturbed symmetric perpendicular distribution $F_o(v_\perp)$ and a perturbed parallel (field aligned) distribution $g(z,u,t)$,

$$f(\vec{r},\vec{v},t) = F_o(v_\perp)g(z,u,t), \tag{2}$$

where $\vec{v} = \vec{v}_\perp + \hat{z}u$, and $|\vec{v}_\perp| = v_\perp$.

2.1 Perturbation Analysis

We proceed with a perturbation calculation correct to order $|\vec{E}|^2$. Equation (2) is therefore expanded according to

$$f(\vec{r},\vec{v},t) = f_o(\vec{r},\vec{v}) + f_1(\vec{r},\vec{v},t) + f_2(\vec{r},\vec{v},t) + \ldots . \tag{3}$$

The spatially dependent equilibrium distribution is

$$\begin{aligned} f_o(\vec{r},\vec{v}) &= F_o(v_\perp)g_o(u)n_o(z), \\ n_o(z) &= N_o(1 - z/L_n), \end{aligned} \tag{4}$$

where a linear profile is assumed around the region of interest, and N_o is the density at the plasma resonance ($z = 0$). The normalization conditions for

the zero order distribution are $\int du\ g_o(u) = 1$ and $\int d^2v_\perp F_o(v_\perp) = 1$. Symmetry in the perpendicular direction also implies that $\int d^2v_\perp \vec{v}_\perp F_o(v_\perp) = 0$. The first order perturbed distribution oscillating at frequency ω_o is

$$f_1(\vec{r},\vec{v},t) = F_o(v_\perp)[g_1(z,u)\exp(-i\omega_o t) + c.c.]$$

and represents the linear response of the plasma. The second order perturbed distribution function contains both a time independent term, corresponding to the modification of the equilibrium by the resonant field, and a second harmonic response

$$f_2(\vec{r},\vec{v},t) = F_o(v_\perp)\ \{\delta g_2(z,u) + [g_2(z,u)\exp(-i2\omega_o t) + c.c.]\}.$$

However, for the purpose of the present study, the second harmonic term will not be considered and is subsequently neglected.

The Boltzmann equation is written as

$$\{\frac{\partial}{\partial t} + u\frac{\partial}{\partial z} - \frac{e}{m}\left[\hat{z}E_\parallel(z)\exp(-i\omega_o t) + \frac{\vec{v}_\perp x \hat{z} B_o}{c}\right]\cdot\nabla_{\vec{v}}\}\ F_o(v_\perp)g(z,u,t) = \left(\frac{\partial f}{\partial t}\right)_{coll}. \quad (5)$$

The unperturbed equilibrium is determined by

$$u\frac{\partial n_o(z)}{\partial z}\, g_o(u)F_o(v_\perp) = \left(\frac{\partial f}{\partial t}\right)_{coll,o}, \quad (6)$$

which states that the plasma density gradient is determined by a balance between the sources and the transport mechanisms, both plasma and atomic, existing in the ionosphere (i.e., elastic and inelastic collisions, ionization, and recombination processes) and contained in the term $\left(\frac{\partial f}{\partial t}\right)_{coll,o}$. Since the present study aims to resolve the acceleration mechanisms in the neighborhood of plasma resonance, a linear approximation (4) for the

unperturbed density profile is made, with the scalelength given by

$$L_n = \left[\frac{1}{n_o}\frac{\partial n_o}{\partial z}\right]^{-1}. \tag{7}$$

The first order parallel distribution function is obtained from (5) by integrating over perpendicular velocities

$$\frac{\partial g_1(z,u)}{\partial z} - i\kappa g_1(z,u) = \frac{en_o(z)E_\parallel(z)}{mu}\frac{\partial g_o(u)}{\partial u}, \tag{8}$$

where $\kappa = \dfrac{\omega_o + i\nu(u)}{u}$, and the first order linearized contribution of the right-hand side term in (5) is approximated by $-\nu(u)g_1(z,u)$, $\nu(u) = \int d^2v_\perp \nu(\vec{v})F_o(v_\perp)$ is the slowing down rate for electrons with velocity u averaged over perpendicular velocities (not to be confused with the average collision frequency for bulk electrons ν_e). Equation (8) is a linear differential equation in z which is integrated along its characteristics. Separating right-going $[g_1^+(z,u)]$ from left-going $[g_1^-(z,u)]$ particles:

$$g_1^\pm(z,u,t) = \frac{e}{mu}\frac{\partial g_o^\pm(u)}{\partial u}\int_{-\infty}^{\infty}\frac{dk}{2\pi i}\frac{\tilde{E}(k)\exp[i(kz - \omega_o t)]}{(k - \kappa)}\cdot \left[n_o(z) - \frac{iN_o}{(k-\kappa)L_n}\right], \tag{9}$$

where $\tilde{E}(k)$ is the Fourier transform of the field $E_\parallel(z)$, and in general $g_n(u) = g_n^+(u)\theta(u) + g_n^-(u)\theta(-u)$, $\theta(u)$ being the Heaviside unit step function.

Carrying out the analysis to second order in the resonant field, the time averaged component of (5) integrated over perpendicular velocities is written as:

$$u \frac{\partial}{\partial z} \delta g_2(z,u) - \frac{e}{m} \left[E_\parallel(z) \frac{\partial g_1^*(z,u)}{\partial u} + E_\parallel^*(z) \frac{\partial g_1(z,u)}{\partial u} \right] = \int d^2 v_\perp \left\langle \left(\frac{\partial f}{\partial t}\right)_{coll,2} \right\rangle, \tag{10}$$

where the time-averaged second order distribution is $\langle f_2(z,\vec{v},t)\rangle = \delta g_2(z,u) F_o(v_\perp)$, and $\langle (\frac{\partial f}{\partial t})_{coll,2} \rangle$ represents the time-averaged second order collisional processes. The interaction between the particles and the resonant electric field $E_\parallel(z)$ occurs within a spatially localized region Δz_i (see Figure 1) that is assumed to be much smaller than the slowing down length $L(u) = u/\nu(u)$ for velocities of interest. In the ionosphere's F region and the upper E region, this assumption is well justified. However, for lower altitudes, the stopping distance decreases with increasing neutral density and this assumption can breakdown. It is also understood that the density scalelength is also large, hence we write

$$L_n, L(u) >> |\Delta z_i| . \tag{11}$$

For distances from the resonant layer $z < L(u)$, $\delta g_2(z,u)$ can be obtained by neglecting the effect of collisions, i.e., the right-hand side of (10), and we can write:

$$\delta g_2^{\pm}(z,u) = \frac{\omega_p^2(z)}{16\pi^3 mu} \frac{\partial}{\partial u} \left\{ \frac{1}{u} \frac{\partial g_o^{\pm}(u)}{\partial u} \int_{-\infty}^{\infty} dk \frac{\tilde{E}^*(k)}{(k-\kappa^*)} \int_{-\infty}^{\infty} dk' \frac{\tilde{E}(k')}{(k'-k)} \exp\left[iz(k-k')\right] \cdot \left[1 + \frac{iN_o/n_o(z)}{(k-\kappa^*)L_n} - \frac{iN_o/n_o(z)}{(k'-k)L_n}\right] + c.c. \right\}. \tag{12}$$

In deriving (12), we have made the approximation that $L(u) \to \mp \infty$ for $\delta g_2^{\pm}$. This approximation is in accordance with (11), which expresses the localized nature of $E_{\parallel}(z)$. Furthermore, since $L_n >> |\Delta z_i|$, the last two terms in (12) make a small contribution, and can thus be neglected.

Up to this point, no specific form has been assumed for either $g_o^{\pm}(u)$ or $\tilde{E}(k)$ except, of course, that they must be physical (i.e., that they are well behaved at infinity). More specifically, we have stated that $E_{\parallel}(z)$ is a spatially localized field near the plasma resonance region, which implies that its Fourier spectrum $\tilde{E}(k)$ is broadband. This being the case, if we further require that the spectral amplitude $|\tilde{E}(k)|$ of the electric field is an entire function (i.e., does not have singularities in the finite k-plane) then, for this second order analysis, one can average the effect of the phases by calculating $\delta g_2(z,u)$ in the asymptotic region where $z \geq z_o >> \Delta z_i$ (see Figure 1). Equation (12) reduces to a single integral

$$\delta g_2^{\pm}(z,u) = \pm \frac{\omega_p^2(z)}{16\pi^2 mu} \frac{\partial}{\partial u} \left[\frac{1}{u} \frac{\partial g_o^{\pm}(u)}{\partial u} \int_{-\infty}^{\infty} \frac{dk \, |\tilde{E}(k)|^2}{i(k-\kappa)} + c.c \right]. \qquad (13)$$

Using (12) or (13), the total time-averaged electron distribution correct to second order is:

$$\langle f^{\pm}(z,\vec{v},t) \rangle = \left[n_o(z) g_o^{\pm}(u) + \delta g_2^{\pm}(z,u) \right] F_o(v_{\perp}). \qquad (14)$$

2.2 Electrostatic Field Structure

To give a concrete example of the changes that occur in the electron distribution, we consider two field patterns, the Airy function and the Lorentzian. These two field structures are characteristic of resonantly

excited plasmas. The Airy structure arises when linear mode conversion limits the resonance amplitude excited by an incident electromagnetic wave propagating into a plasma with a density gradient. The Lorentzian pattern replaces the Airy pattern whenever the mean free path of the thermal electrons is smaller than the characteristic Airy scalelength, i.e., $(\bar{v}_e/\nu_e) < L_n(k_D L_n)^{-2/3}$, $\bar{v}_e$ being the electron thermal velocity.

The electric field for an electrostatic plasma wave, propagating along the magnetic field in the positive z direction is given by [Morales and Lee, 1974]

$$E_\parallel(z) = -i\pi E_o(k_D L_n)^{2/3}\left[Ai(-\zeta - i\Gamma') - iGi(-\zeta - i\Gamma')\right], \qquad (15)$$

where $\zeta = (k_D L_n)^{2/3}\, z/L_n$, $\Gamma' = (k_D L_n)^{2/3}\Gamma$, $\Gamma = \nu_e/\omega_o$, Ai and Gi are solutions to Airy's equation given in Abramowitz and Stegun [1965], and E_o is a field amplitude that is related by a mode conversion efficiency to the incident electromagnetic wave power. In the limit where collisions dominate, we obtain the Lorentzian profile

$$E_\parallel(z) = \frac{E_o L_n}{z + i\Gamma L_n}. \qquad (16)$$

It is worth noting that for $z/L_n \lesssim \Gamma$, (15) is approximated to leading order by (16). This effect is illustrated in Figure 2a, which depicts the magnitudes of both the Airy and Lorentzian patterns for two values of the damping factor, $\Gamma' = 0.2$ and 0.8. Figure 2b displays the real parts of both patterns for $\Gamma' = 0.4$. The Lorentzian consists mainly of a single wavelength, that is almost in phase with the Airy pattern near the origin, and travelling down the density gradient. This feature is also found by taking the Fourier transform of both field structures:

$$\tilde{E}_A(k) = 2\pi E_o L_n \theta(k) \exp\left\{-\frac{k}{k_o} - i\left[\frac{(kL_n)^3}{3(k_D L_n)^2} + \frac{\pi}{2}\right]\right\}, \tag{17}$$

$$\tilde{E}_L(k) = 2\pi E_o L_n \theta(k) \exp\left[-\frac{k}{k_o} - \frac{i\pi}{2}\right], \tag{18}$$

where again $\theta(k)$ is the Heaviside unit step function, $\tilde{E}_A(k)$ is the Fourier transform of the Airy pattern of (15) and $\tilde{E}_L(k)$ that of the Lorentzian of (16); the characteristic wavenumber $k_o = \omega_o/a = (\Gamma L_n)^{-1}$, where a is the effective phase velocity of the Lorentzian and/or the Airy envelope. The derivations of (17) and (18) are shown in the Appendix.

The Fourier transforms of (17) and (18) have common features. They are both broadband and unidirectional. In fact, they only differ by a highly oscillatory phase term in the Airy spectrum. The power spectra for the Airy and the Lorentzian are therefore identical. Accordingly, in the limit of second order analysis, a particle passing through either field pattern emerges downstream at $z_o >> \Delta z_i$, away from the interaction region having, on the average, experienced identical effects. The magnitude of the electric field Fourier spectrum is plotted in Figure 3 as a function of both wavenumber k and parallel velocity u, where $k = \omega_o/u$. The resonant field k-components interact with the background electrons and accelerate them. Components varying from zero up to values on the order of $k_o = (\Gamma L_n)^{-1} < k_D$ efficiently interact with the background particles. As k increases, the interaction with the resonant electric field structure decreases until $k \to k_D$, where Landau damping destroys the wave completely. In terms of the velocity space interaction, this translates as acceleration of particles mainly in the tail by an electric field of constant magnitude produced by the plateau that exists in the

exponential behavior of the spectrum from $\bar{v}_e < u \approx a$ up to $u \to +\infty$. For velocities $u < a$, closer to the bulk of the velocity distribution, the field has negligible k-components and particle acceleration is small. As $u \to \bar{v}_e$, Landau damping completely eliminates any k-components.

Substituting for either of the field patterns in (13) gives

$$\delta g_2^+(z,u) = \frac{\omega_p^2(z)(E_o L_n)^2}{2mu} \frac{\partial}{\partial u} \left\{ \frac{1}{u} \frac{\partial g_o^+}{\partial u} e^{-2a/u} \left[\pi \cos \left(\frac{2\nu(u)}{k_o u} \right) \right. \right. \tag{19}$$

$$\left. \left. + \mathrm{Ei}\,(2a/u) \sin \left(\frac{2\nu(u)}{k_o u} \right) \right] \right\}$$

for $u > 0$, and

$$\delta g_2^-(z,u) = \frac{\omega_p^2(z)\,(E_o L_n)^2}{2mu} \frac{\partial}{\partial u} \left[\frac{1}{u} \frac{\partial g_o^-(u)}{\partial u} e^{2a/|u|} \, E_1(2a/|u|) \sin \left(\frac{2\nu(u)}{k_o |u|} \right) \right] \tag{20}$$

for $u < 0$; Ei and E_1 are exponential integral functions defined in Abramowitz and Stegun [1965]. For the case $\nu(u) \to 0$, i.e., negligible slowing down of fast particles, then $\delta g_2^- \to 0$ and

$$\delta g_2^+(z,u) = \frac{\pi\omega_p^2(z)(E_o L_n)^2}{2mu} \frac{\partial}{\partial u} \left[\frac{1}{u} \frac{\partial g_o^+}{\partial u} e^{-2a/u} \right] . \tag{21}$$

No wave particle resonances occur for particles moving up the geomagnetic field (i.e., in the negative z direction) due to the unidirectional nature of the resonant field wavenumber spectrum. If the resonant field spectrum had k components in the direction opposite to the geomagnetic field (negative z direction), then particles with $u < 0$ would be accelerated yielding a non zero δg_2^-.

2.3 Zero Order Distribution

A self-consistent calculation of the zero order distribution function $f_o(z,\vec{v})$ requires the solution of equation (6). We shall not attempt this, however, as it is quite difficult for F region conditions and contributes little to the features we wish to emphasize. Instead, we consider a model characteristic of an equilibrium ionosphere that can simulate different regimes of the ionosphere by changing the value of the parameters. Through this approach, we exhibit the main features contained in the present analysis.

A bi-Maxwellian models the zero order electron distribution and is expressed as

$$g_o(u) = \frac{(1-\Delta)}{\sqrt{\pi}\,\bar{v}_e} e^{-u^2/\bar{v}_e^2} + \frac{\Delta}{\sqrt{\pi}\,v_f} e^{-u^2/v_f^2}, \tag{22}$$

where Δ is the fractional density of the energetic tail, usually of the order of a few percent, $\bar{v}_e$ is the thermal velocity of the bulk plasma, and v_f is the characteristic velocity of the tail. Δ, $\bar{v}_e$, and v_f are free parameters that model the various ionospheric conditions. Using (21) and (22), the resulting total electron distribution function of (14) (accurate to second order) is

$$g(z,u) \simeq \frac{n_o(z)(1-\Delta)}{\sqrt{\pi}\,\bar{v}_e} e^{-u^2/\bar{v}_e^2} + \frac{n_o(z)\Delta}{\sqrt{\pi}\,v_f} e^{-u^2/v_f^2} \cdot \left\{1 + \frac{E_o^2}{E_s^2} e^{-2a/u}\left[1 - \frac{a v_f^2}{u^3}\right]\right\}, \tag{23}$$

where $E_s = \left(\frac{1}{2} m v_f^2\right)/\left(\sqrt{2}\pi e L_n\right)$ is a normalizing field that scales as the average tail energy per unit charge over the density scalelength. If there is no initial tail, i.e., only a single Maxwellian background, then $\Delta = 1$ and

$v_f = \bar{v}_e$. Figure 4 shows a plot of (23) for $\Delta = 0.01$, $v_f = 10\bar{v}_e$, and a resonant field having an effective phase velocity $a = 20\bar{v}_e$. For $E_o = 3E_s$, particles diffuse toward higher velocities causing a swelling of the tail. This tail heating is produced by the power spectrum of the applied electric field $\tilde{E}(k = \omega_o/u)$ displayed in Figure 3. The heating is most significant for large velocities where the spectral density is largest and nearly constant.

Equation (23) shows that the exponentially decaying Gaussian tail of the background is enhanced and spread out by the perturbation term. The larger the amplitude of the applied field, the larger the diffusion toward the tail. However, since there are more particles at lower velocities, one can see that because the magnitude of $\tilde{E}(k)$ increases with velocity (Figure 3), there may be a velocity bin where more particles diffuse into it from the bulk (and more populated) side than there are particles leaving that region toward higher velocities. This effect may produce a localized swelling of the tail that would ultimately cause a bump in the distribution for large enough fields. The region where this process would occur is, of course, a function of both v_f and a, i.e., the tail and the resonant field's effective phase velocities, respectively. The condition for bump production is analyzed in the following section.

2.4 Threshold for Bump Production

We now investigate the condition for producing a region of positive slope in the distribution function of (23). For $\frac{\partial g(z,u)}{\partial u} \geq 0$, one must satisfy the condition

$$\frac{E_o^2}{E_s^2} \geq \frac{\exp(2a/u)}{\left[\frac{3av_f^4}{2u^5} - \left(1 - \frac{av_f^2}{u^3}\right)^2\right]} \quad . \tag{24}$$

Again, for the case of a single Maxwellian plasma, a similar expression is obtained with $v_f = \bar{v}_e$. Positive slopes will occur on the distribution only in the region where the denominator of (24) is positive, i.e., whenever

$$\left[\frac{a}{u} - \left(\frac{3a}{2u}\right)^{1/2}\right] < (u/v_f)^2 < \left[\frac{a}{u} + \left(\frac{3a}{2u}\right)^{1/2}\right]. \tag{25}$$

It should be emphasized that although the positive slope condition of (24) is calculated for the specific spectra of the Airy and the Lorentzian field structures, this method is applicable in general to any spectrum satisfying the conditions leading to (13). In this case, the condition of (24) for a positive slope in the tail distribution is generalized to

$$\frac{A^2}{E_n^2} \geq \frac{2}{\left[-\frac{v_f^4}{4u^2} G''(u) + \frac{v_f^2}{u}\left(1 + \frac{v_f^2}{4u^2}\right) G'(u) - G(u)\right]} \quad , \tag{26}$$

where

$$G(u) = \frac{1}{A^2 w^2}\left[\int_{-\infty}^{\infty} \frac{dk}{2\pi i} \frac{|\tilde{E}(k)|^2}{(k - \kappa)} + c.c.\right],$$

$$E_n = \frac{\frac{1}{2}mv_f^2}{ew} \quad ,$$

A is the amplitude of the applied field, and w its characteristic width. It can be shown that for a Lorentzian or an Airy pattern (26) reduces to (24).

2.5 Sideband Emissions

2.5.1 Threshold for Growth

The existence of a positive slope in the distribution suggests that plasma waves with phase velocities resonant with particles in the positive slope region can become unstable. These unstable plasma waves form broad sidebands in the neighborhood of the main frequency ω_o. For sideband amplification, the field E_o must be large enough not only to produce a positive slope in the distribution, but also to overcome collisional and Landau damping. This condition is written as

$$\frac{\gamma}{\omega_o} \simeq \frac{\pi}{2} \frac{\omega_r u^2}{\omega_o (1 + 6\bar{v}_e^2/u^2)} \frac{\partial g(u)}{\partial u} \Bigg|_{u = \omega_r/|k|} - \Gamma > 0 \qquad (27)$$

where the sideband frequency is $\omega_s = \omega_r + i\gamma$, and we assume $\gamma \ll \omega_r$. Equation (27) is accurate to order $(\bar{v}_e^4/u^4)$. From (23), the condition of (27) is rewritten as:

$$\frac{E_o^2}{E_s^2} \geq \frac{\exp(2a/u)\left[1 + \frac{\Gamma(\omega_o/\omega_r)(v_f/u)^3 (1 + 6\bar{v}_e^2/u^2)}{\sqrt{\pi}\,\Delta} \exp(u^2/v_f^2)\right]}{\left[\frac{3av_f^4}{2u^5} - \left(1 - \frac{av_f^2}{u^3}\right)^2\right]}, \qquad (28)$$

where again in the case of a single Maxwellian plasma $\Delta \to 1$ and $v_f = \bar{v}_e$. Comparing (28) to (24), one concludes that the addition of the term proportional to Γ in the former increases the wave growth threshold over the threshold for positive slope. In practice, however, the term containing Γ in (28) is usually small compared to unity in the square brackets.

Given a certain field E_o above the instability threshold of (28), we expect growth of sideband waves with growth rates given by (27). The growth rate is largest for the sideband whose phase velocity matches the largest positive slope, and decreases away from this value for both larger and smaller velocities up to frequencies with phase velocities which correspond to negative slope on the distribution.

2.5.2. Sideband Frequency Spectrum

The frequencies of the growing sidebands can be determined in the case of a homogeneous medium, from the dispersion relation. For phase velocities larger than the background thermal velocity, the dispersion relation for Bohm-Gross waves is approximately

$$\omega_s^2 \simeq \omega_p^2/(1 - 3\bar{v}_e^2/u^2), \tag{29}$$

where it is assumed that ω_s is real. Velocities in the positive slope region usually satisfy the condition $u \lesssim a$, while the Airy electric field structure at plasma resonance satisfies the relation

$$\omega_o^2 \simeq \omega_p^2/(1 - 3\bar{v}_e^2/a^2). \tag{30}$$

With $u \lesssim a$, equations (29) and (30) indicate that sidebands should be radiated at frequencies $\omega_s \gtrsim \omega_o$, i.e., larger than the initial resonant frequency. Note that for the Lorentzian (cold plasma), the phase velocity is infinite at resonance, so that the preceeding statement is still correct. The wavenumbers corresponding to these waves are obtained by the condition $k_s = \omega_s/u$.

For the case of an inhomogeneous plasma, recall that the distribution given in (23) is valid in the spatial range $z_o \leq z < L(u)$, where z_o is an arbitrarily chosen location satisfying the condition $z_o >> \Delta z_i$ (Figure 1). Equation (29) is therefore rewritten using the position-dependent plasma frequency:

$$\omega_p^2(z) = \omega_p^2(o)\,(1 - z/L_n), \tag{31}$$

where $\omega_p(o) = \omega_p$. Therefore, in the inhomogeneous plasma, although the sideband waves have the same phase velocities as in the homogeneous case, i.e., in the range $u \lesssim a$, their frequencies are smaller because $\omega_p(z) < \omega_p(o)$. As a result, the spectrum of the sidebands is shifted to lower frequencies than for a comparable homogeneous case, as is clear from (29).

The sideband frequency spectrum is therefore determined by two factors, namely, that the bump occurs at velocities $u \lesssim a$, and the plasma frequency decreases away from the resonance region. Furthermore, since the perturbed distribution is valid at any z satisfying the condition $z_o \leq z < L(u)$, sidebands should be amplified for all z's in this range at frequencies satisfying the local dispersion relation. Backscattered Thomson radar returns would therefore see sidebands caused by the integrated effect from the different heights. The recorded frequency spectrum would manifest itself as a bump-like distribution of broadband frequencies that spread around the initial frequency ω_o, depending on the prevailing ionospheric and resonant field parameters ($\bar{v}_e$, v_f, a, z_o, L_n, . . .).

We have given a simple argument to the effect of the inhomogeneity on the generated sidebands. However, the instability should be treated using a fully spatially dependent analysis. Rather than using an initial value treatment of

the instability, a boundary value approach would be more appropriate, as the instability is convective rather than absolute. One should note that an exact comparison between our theory and the experimental results of Starke and Malmberg [1978] is only valid in this limit. However, even with this simple approach, one can see the similarities between the broad sidebands they measure and the ones we calculate. One could also note a similarity between the sidebands of the present analysis and the "broad bump" in the plasma line spectrum observed by Thomson radar returns [Showen and Kim, 1978] during ionospheric heating experiments. In this experiment, the wavelength of the Thomson radar is fixed, therefore, the broad bump is made of only those sidebands that match with the radar wavenumber. The recent rocket experiment of Rose, et al. [1985], also shows evidence of broad sideband Langmuir waves around the heater frequency ω_o measured on the upleg of the rocket trajectory, below the reflection layer.

3. DISCUSSION

The second order analysis presented in this work has shown that the nonlinear modification of the background distribution function by a resonant electrostatic field may cause tail heating, bump production, and broad sideband emissions. The power levels necessary to trigger these effects in the ionosphere's E and F regions are illustrated by the following example. Assuming the same background conditions as for Figure 4, i.e., $\Delta = 0.01$, $v_f = 10\bar{v}_e$, $a = 20\ \bar{v}_e$, $\bar{v}_e = 0.15$ eV, and $\Gamma \sim 10^{-5}$. The resulting distribution is plotted in Figure 5a for three cases; namely, $E_o = 0$, $3E_s$, and $6E_s$, where $E_s = 3.39/L_n$ (in SI units) for the preceeding parameters. The threshold conditions for both positive slope [Equation (24)] and growth [Equation (28)] are plotted in Figure 5b and appear as one curve since the two plots are almost superimposed, showing that for F region parameters, the threshold for growth is not much larger than that for positive slope. Outside the region contained within the dotted lines, the condition of (25) is not satisfied and the denominators of both (24) and (28) become negative precluding the formation of a positive slope in these regions. The minimum point on the curve of 5b is determined numerically because the functions involved are transcendental. In this example, one finds $E_{o,thr} = 4.83E_s$. Therefore, for the plotted value of $E_o = 6E_s$, one is well above threshold, and a bump does develop. The growth rate corresponding to this value of E_o and obtained from (27) is plotted in figure 5c, where it is clear that growth (i.e., $\gamma > 0$) occurs only in the region where the distribution has a positive slope, and that it maximizes at the velocity where the slope is maximum in the distribution. Velocities where $\gamma < 0$, correspond to damped waves. Assuming ω_o to be of the order of few MHz, which is usually the case for overdense heating of both E and F regions in the ionosphere, the rise time for the

instability is only a few hundred microseconds. Frequencies at the edges of the sideband grow at slower rates. In Figure 5d, curve a shows the width $\Delta\omega_s$ of the sidebands spectrum produced for a homogeneous medium using (29), $z = 0$. One may extend the validity of curve a to an inhomogeneous medium with a very large density scalelength such that $z/L_n \ll 1$. Curve b shows the other limit case wherein $z/L_n = 0.1$, a finite value which makes the condition $z < L(u)$ just valid for the ionospheric plasma. It should be kept in mind that at each value of z, such that $\Delta z_i \ll z < L(u)$, the distribution function with the bump exists and sidebands are being produced. This means that curves a and b in Figure 5d should not be viewed as two discrete cases, but rather as two bounds for the possible spread of sidebands ($\delta\omega_s$) that this particular example would generate.

To justify the value of z used to generate curve b of Figure 5d in terms of slowing down length, we mention that for energies U(u) of the electrons being considered, which vary usually form a few to a few hundred electron volts, the slowing down length L(u), evaluated using the continuous slowing down approximation where $L(u) = U/(-dU/dz)$, has a minimum value that varies from a few kilometers near the ionosphere's upper E region to over a few hundred kilometers in the F region. This result is displayed in Figure 6 which incorporates all the important slowing down processes present in the ionosphere's upper E and F regions. Density scalelengths, on the other hand, vary from a few kilometers in the E region to one hundred kilometer in the F region. Therefore, a value of $z \sim 0.1\ L_n < L(u)$ is reasonable for an upper range of validity of the distribution with the bump.

Since the ionosphere is a highly variable medium, we present in Table 1 the different scalelength dependent parameters. For the resonant field's

effective phase velocity we assume, $a = \nu_e L_n = 20\bar{v}_e$, there exists different combinations for the product ($\nu_e L_n$). Since both the ionospheric density scalelength and the bulk electron collision rate depend upon altitude and local time, we compute the threshold parameters for different combinations of ν_e and L_n. The quantities calculated in Table 1 use the same parameters that are used in generating the previous figures. Typical values of ν_e and L_n in the ionosphere's upper E and F regions have a product that varies around the value chosen in the present example.

For a given threshold field ($E_{o,thr}$), there exists a corresponding energy flux density for the electrostatic wave P_{es} that is related to power delivered by the high frequency electromagnetic waves at the reflection layer P_{HF}. In Table 1, P_{HF} is estimated assuming a mode conversion efficiency, $\eta = P_{es}/P_{HF} = 15\%$. That is, P_{HF} is the necessary power density needed at the reflection layer (usually anywhere between 100 Km and 350 Km altitude) in order to produce an electrostatic field just above the threshold value. The values displayed in Table 1 are to be compared with vacuum power densities of 0.50 mW/m^2 delivered at 250 Km altitude by the Tromso Heating facility [Stubbe, et al., 1982], 0.15 mW/m^2 by the Alaska HIPAS facility [Wong, et al., 1983], and 0.05 mW/m^2 by the Arecibo heater [Mantas, et al., 1981]. For the example we are presenting, as well as most other cases, the thresholds for instability are within these values.

It is also of interest to compare the thresholds for bump instability that we have calculated with those necessary to produce parametric instabilities, another second order nonlinear process commonly encountered during ionospheric modification experiments. The two mechanisms pertinent to this

situation would be the decay instability with the electromagnetic pump decaying near its cutoff into a plasma wave and an ion acoustic wave, and the oscillating two stream instability involving a purely growing ion mode. The threshold estimated for the decay instability in the ionosphere [Fejer, 1979] corresponds to an HF pump amplitude of 0.25 V/m or a vacuum HF power $P_{HF} = 180\mu W/m^2$ for F region parameters. For the oscillating two stream instability, the threshold is even higher. This implies that the sideband instability thresholds calculated are less than, and at most on the order of, the smallest parametric instability threshold, namely the decay process.

4. CONCLUSIONS

The second order analysis presented has shown the following major effects in response to the excitation of a spatially localized electric field parallel to the earth's magnetic field.

1) For the two field structures "typical" of a plasma resonance, the wavenumber spectrum is broadband and unidirectional. The power spectra of both the Airy and the Lorentzian structures are identical, i.e., in the second order time averaged limit, the asymptotic modifications in the distribution function are identical. However, one should note that the Airy pattern has, in addition, oscillating structures in it. Its equivalence to the Lorentzian is therefore limited to situations where its damped envelope is the main contribution to the interaction, which is the case in the present second order analysis. Under different conditions, the oscillating part of the Airy structure could be responsible for other types of interactions not considered here (e.g., particle trapping).

2) Particle acceleration caused by direct plasma resonance electric fields (with unidirectional k-spectrum) occurs only for particles impinging from high altitude as is clearly evident from (21). No up going particles are resonantly accelerated by such a field. This result implies that any experimental evidence for fast particle acceleration upstream from the resonance layer indicates either strong pitch angle scattering or the existence of electric fields not produced by direct plasma resonance but rather by some other mechanism, like parametric instabilities.

3) The tail of the electron distribution is heated producing an enhanced fast electron flux in the range from a few eV to few hundred eV. The low energy part of this tail could be responsible for the observation of enhanced airglow at 6300Å and 5577Å [Sipler and Biondi, 1972], and may account for the high energy particles that are also observed [Carleson, Wickwar, and Mantas, 1982].

4) Present day ionospheric heating experiments appear to deliver powers that are large enough to overcome the threshold for bump formation. Therefore, a bump is expected to develop in the tail of the distribution function. Also, it is found that for the ionosphere, this threshold is quite close to the wave instability threshold, so that enhanced noise levels should also occur.

5) Broad sidebands are generated in the F region by the bump instability, their growth time is of the order of 10^{-1} millisecond. They are produced at different heights downstream from the interaction region, up to the slowing down length or nonlinear saturation length, whichever is shortest. For a distant observer, the net broad sideband spectrum consists of the integrated effect from all these heights. Experiments measuring the plasma line spectrum using Thomson radar backscattering from the ionosphere during HF heating [Kantor, 1974; Showen and Kim, 1978], show evidence, under some conditions, of a "broad bump" in the spectrum. In addition, the broad spectrum of plasma waves around the HF heater frequency measured in the HERO rocket flights [Rose, et al., 1985], could be another example of the phenomena considered by the present study.

In the laboratory, the results of Starke and Malmberg [1978] have simularities to ours, both in the broad sideband spectrum they find and in the quasilinear theory they invoke. However, since the spatial dependence of the growing sidebands is not self-consistently included in our analysis, a direct comparison is not possible at this point.

APPENDIX: FOURIER TRANSFORMS OF THE AIRY PATTERN AND THE LORENTZIAN

We derive here equations (17) and (18). The Fourier transform is defined as:

$$\tilde{E}(k) = \int_{-\infty}^{\infty} dz\, E_{\parallel}(z)\, \exp(-ikz) \tag{A1}$$

where $E_{\parallel}(z)$ is defined by (15) for the Airy pattern and (16) for the Lorentzian.

One may write (15) as [Abramowitz and Stegun, 1965]

$$E_{\parallel}(z) = E_o(k_D L_n)^{2/3} \int_0^{\infty} dt\, \exp\left\{-i\left[\frac{t^3}{3} + (k_D L_n)^{2/3}\left(-\frac{z}{L_n} - i\Gamma\right) t + \frac{\pi}{2}\right]\right\}. \tag{A2}$$

Substituting in (A1) and integrating over all space

$$\tilde{E}_A(k) = 2\pi E_o (k_D L_n)^{2/3} \int_{-\infty}^{\infty} dt\, \exp\left\{-i\left[\frac{t^3}{3} - (k_D L_r)^{2/3}\Gamma t + \frac{\pi}{2}\right]\right\} \cdot \delta[k - \alpha t]$$

$$= 2\pi E_o L_n \exp\left[-k/k_o - i\left(\frac{k^3}{3\alpha^3} + \frac{\pi}{2}\right)\right], \quad k > o \tag{A3}$$

$$= 0 \qquad , \quad k < o \tag{A4}$$

where $k_o = (\Gamma L_n)^{-1}$, $\alpha = (k_D L_n)^{2/3}/L_n$, and k_D is the Deybe wavenumber. Equations (A3) and (A4) are identical to (17).

For the Lorentzian case, (A1) is rewritten as

$$\tilde{E}_L(k) = \int_{-\infty}^{\infty} dz\, \frac{E_o L_n}{z + i\Gamma L_n} \exp(-ikz)$$

$$= 2\pi\, E_o L_n \exp(-k/k_o - i\pi/2), \quad k > 0 \tag{A5}$$

$$= 0 \qquad , \quad k < 0 \tag{A6}$$

where the integration is carried out in the complex z plane closing the contour in the lower half-plane for $k > 0$ (encircling the pole at $-i\Gamma L_n$), and in the upper half-plane for $k < 0$ (where no poles are enclosed). Again, equations (A5) and (A6) are identical to (18).

ACKNOWLEDGMENTS

The authors would like to thank Miss Aileen Wang for her help in computing the slowing down rates for energetic electrons in the ionosphere. This work is supported by the Office of Naval Research.

REFERENCES

Abramowitz, M., and I.A. Stegun (eds.), Handbook of Mathematical Functions, pp. 228 and 446, Dover Publications Inc., New York, 1965.

Carleson, H.C., V.B. Wickwar, and G.P. Mantas, Observations of fluxes of superthermal electrons accelerated by HF excited instabilities, J. Atmos. Terr. Phys., 44, 1089, 1982.

Fejer, J.A., Ionospheric modification and parametric instabilities, Rev. Geophys. Space Phys., 17, 135, 1979.

Haslett, J.C., and L.R. Megill, A Model of the enhanced airglow excited by RF radiation, Radio Sci., 9, 1005, 1974.

Kantor, I.J., High frequency induced enhancements of the incoherent scatter spectrum at Arecibo, 2, J. Geophys. Res., 79, 199, 1974.

Mantas, G.P., H.C. Carleson, and C.H. LaHoz, Thermal response of the F region ionosphere in artificial modification experiments by HF radio waves, J. Geophys. Res., 86, 561, 1981.

Meltz, G., L.H. Holway, and N.M. Tomljanovich, Ionospheric heating by powerful radio waves, Radio Science, 9, 1049, 1974.

Mjølhus, E., Linear conversion in a magnetized plasma with density gradient parallel to the magnetic field, J. Plasma Phys., 30, 179, 1983.

Morales, G.J., and Y.C. Lee, Ponderomotive-Force effects in a nonuniform plasma, Phys. Rev. Lett., 33, 1016, 1974.

Rose, G., B. Grandel, E. Neske, W. Ott, K. Spenner, J. Holtet, K. Måseide, and J. Trøim, Experimental Results from the HERO Project: In situ measurements of ionospheric modifications using sounding rockets, J. Geophys. Res., 90, 2851, 1985.

Shoucri, M., G.J. Morales, and J.E. Maggs, Ohmic heating of the polar F region by HF pulses, J. Geophys. Res., 89, 2907, 1984.

Showen, R.L., and D.M. Kim, Time variations of HF-induced plasma waves, J. Geophys. Res., 83, 623, 1978.

Sipler, D.P. and M.A. Biondi, Measurements of the $O(^1D)$ quenching rate in the F region, J. Geophys. Res., 77, 6202, 1972.

Stammes, K., and M.H. Rees, Inelastic scattering effects on photoelectron spectra and ionospheric electron temperature, J. Geophys. Res., 88, 6301, 1983.

Starke, T.P., and J.H. Malmberg, Experiment on sideband dispersion, Phys. Fluids, 21, 2242, 1978.

Stubbe, P. H. Kopka, H. Lauche, M.T. Rietveld, A. Brekke, O. Holt, T.B. Jones, T. Robinson, Å. Hedberg, B. Thidé, M. Crochet, and H.J. Lotz, Ionospheric modification experiments in northern Scandinavia, J. Atmos. Terr. Phys., 44, 1025, 1982.

Wong, A.Y., G.J. Morales, D. Eggleston, J. Santoru, and R. Behnke, Rapid conversion of electromagnetic waves to electrostatic waves in the ionosphere, Phys. Rev. Lett., 47, 1340, 1981.

Wong, A.Y., J. Santoru, C. Darrow, W. Lang, and J.G. Roederer, Ionospheric Cavitons and Related Nonlinear Phenomena, Radio Sci., 18, 815, 1983.

FIGURE CAPTIONS

Figure 1. Schematic diagram illustrating the geometry of the problem. Electrons from the high density side (on the left) pass through the localized interaction region at plasma resonance ($z = 0$), having a characteristic width Δz_1. They emerge accelerated in the region $z_o \leq z \ll L(u)$ forming an enhanced tail and, above a threshold level, a bump in the distribution. The bump eventually relaxes to the equilibrium background distribution (on the far right) after a distance longer than a slowing down length $L(u)$.

Figure 2. Spatial dependence of resonant parallel electric fields for the Airy (continuous lines) and the Lorentzian (dashed lines) patterns for different damping values: (a) Magnitudes for $\Gamma' = 0.2$ and 0.8; (b) Real parts for $\Gamma' = 0.4$. Note the wavelike structure of the Lorentzian in the neighborhood of the origin.

Figure 3. Dual plot of the magnitude of the Fourier transformed field (for either the Airy or the Lorentzian pattern) versus wavenumber k (upper scale and dashed curve), and versus velocity $u = \omega_o/k$ (lower scale and continuous curve). Normalization is such that $k_o = \omega_o/a = (\Gamma L_n)^{-1}$, a is the effective phase velocity of the resonant field.

Figure 4. Modification in electron velocity distribution obtained from equation (22) for $E_o = 3E_s$, $a = 2v_f = 20\bar{v}_e$, and $\Delta = 1\%$. Unperturbed background distribution ($E_o = 0$) is plotted for comparison.

Figure 5. Production of a bump in the distribution function and associated

sideband instability: (a) the distribution function with the tail magnified (scale to the right) for $a = 2v_f = 20\bar{v}_e$, $\bar{v}_e \sim 0.15$ eV, $\Delta = 1\%$, $\omega_o/2\pi \sim 5$ MHz, $\Gamma \sim 10^{-5}$, and different values of E_o; (b) threshold curves for bump formation and instability generation (both curves superimposed); (c) temporal growth rates for the unstable sidebands ($\gamma > 0$) generated on the positive slope region of the bump for $E_o = 6E_s$; (d) frequency range $\Delta\omega_s$ corresponding to sidebands generated locally in a slowly varying medium for curve a: $z = 0$, and curve b: $z = 0.1L_n$. A distant observer downstream from the resonance region may sample sidebands within a frequency range $\delta\omega_s$.

Figure 6. Energy dependence of slowing down length L(u) for fast electrons in the upper E region (at 150 Km altitude) and the F region (at 300 Km altitude). Estimates are based on a model incorporating the most dominant slowing down mechanisms of the ionosphere: impact excitations, ionizations, recombinations, electron-electron collisions, . . . [see, for example, Stammes and Rees (1983) and the references therein]. The background ionosphere used is the one given by Shoucri, Morales, and Maggs [1984].

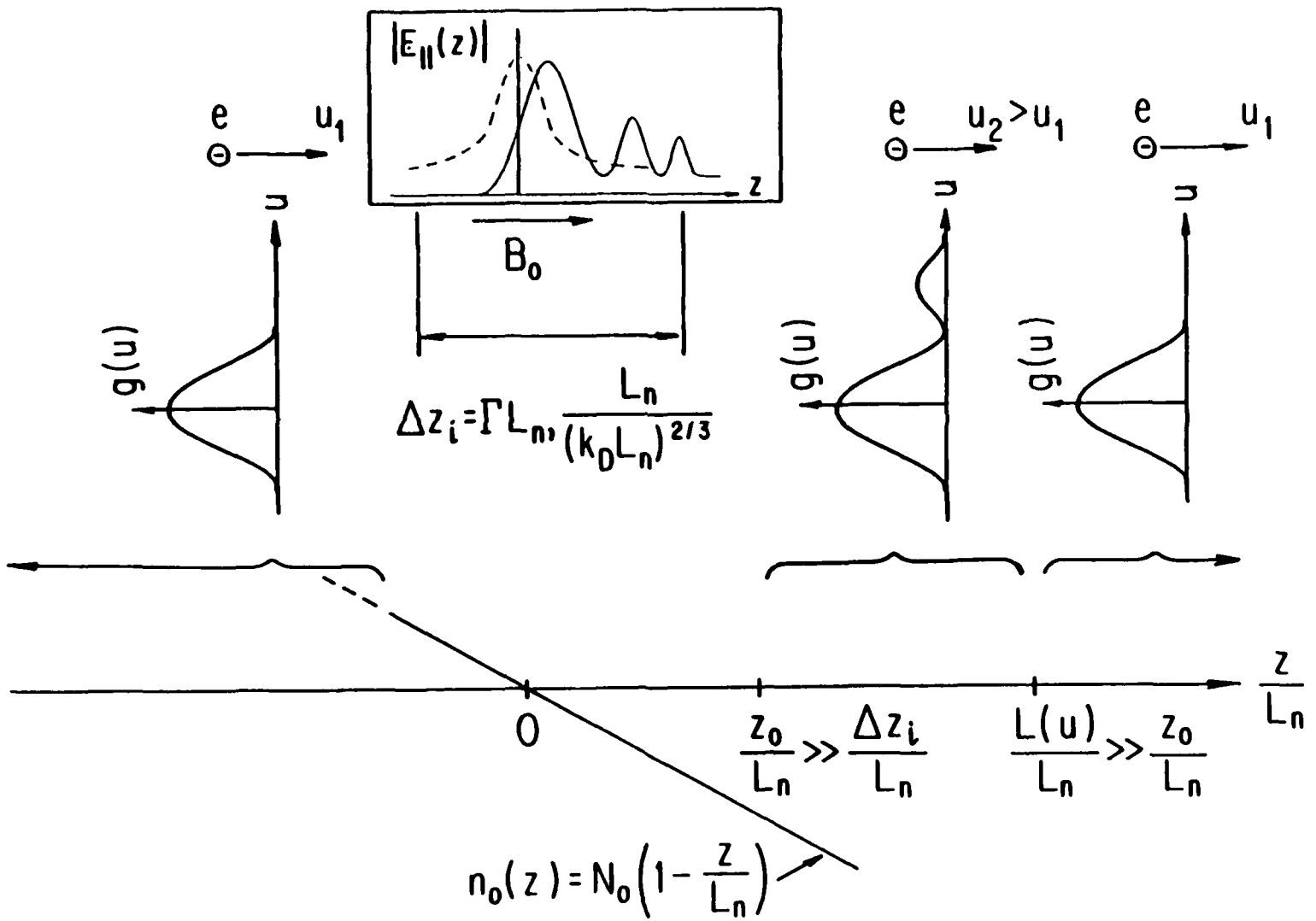
$|E_{\parallel}(z)|$
z
e
u_1
$u_2 > u_1$
B_0
n
g(u)
$\Delta z_i = \Gamma L_n \frac{L_n}{(k_D L_n)^{2/3}}$
0
$\frac{z_0}{L_n} \gg \frac{\Delta z_i}{L_n}$
$\frac{L(u)}{L_n} \gg \frac{z_0}{L_n}$
$\frac{z}{L_n}$
$n_0(z) = N_0\left(1 - \frac{z}{L_n}\right)$

Figure 1

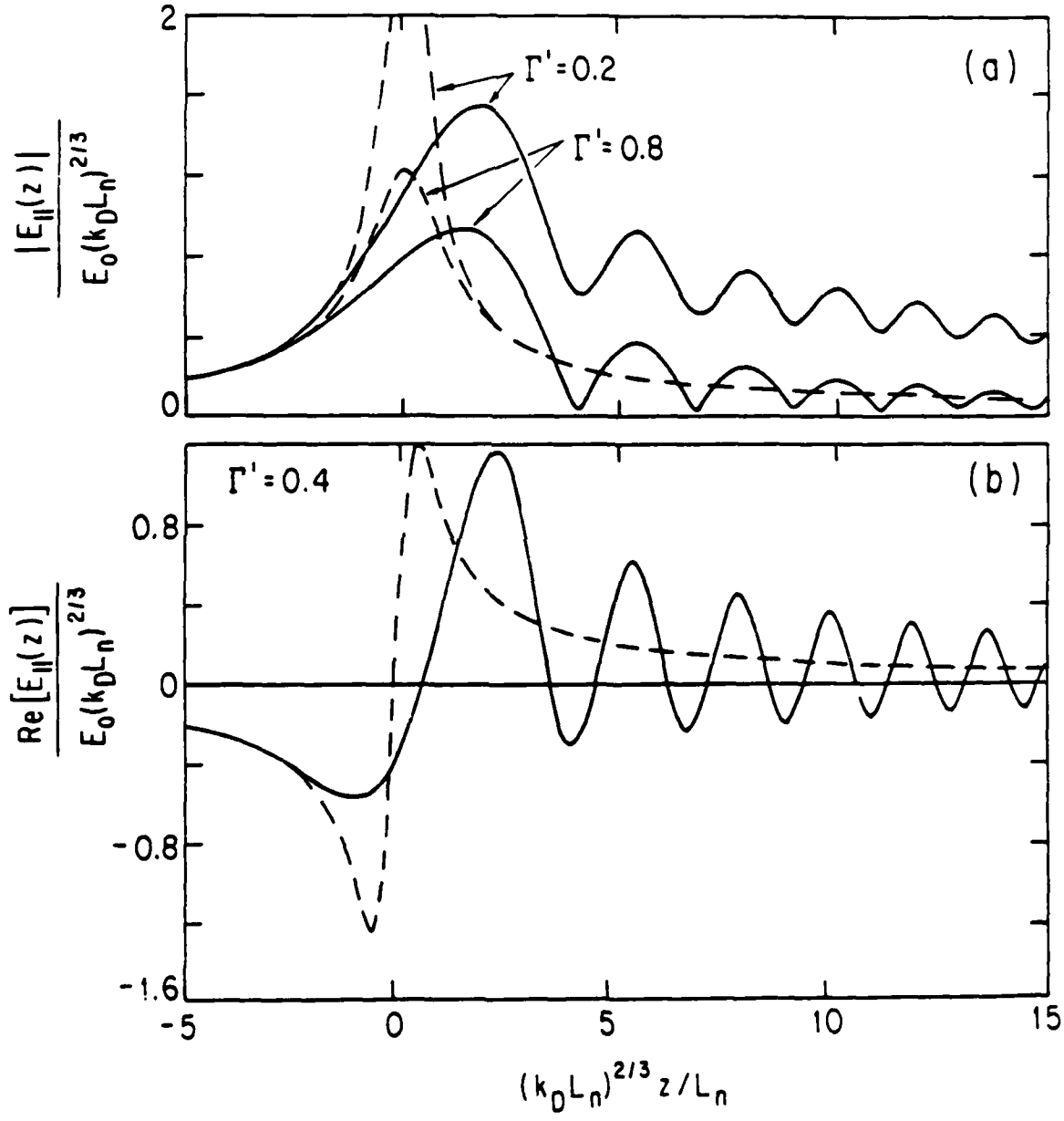
2
0
Γ'=0.2
Γ'=0.8
(a)
$\frac{|E_{\parallel}(z)|}{E_0(k_D L_n)^{2/3}}$
Γ'=0.4
(b)
0.8
0
-0.8
-1.6
$\frac{Re[E_{\parallel}(z)]}{E_0(k_D L_n)^{2/3}}$
-5
0
5
10
15
$(k_D L_n)^{2/3} z/L_n$

Figure 2

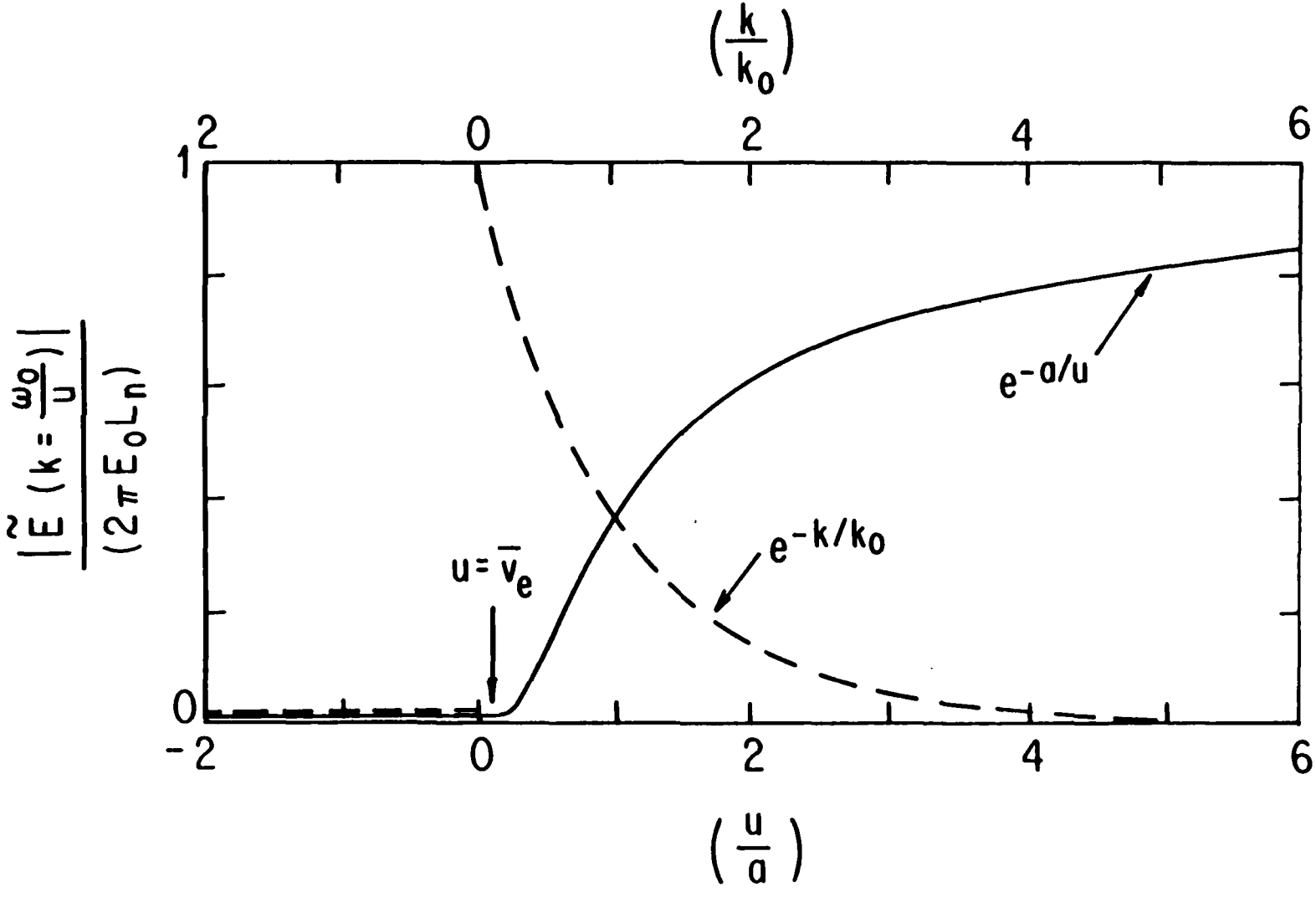
$\left(\frac{k}{k_0}\right)$
2
0
2
4
6
1
$\frac{|\tilde{E}(k=\frac{\omega_0}{u})|}{(2\pi E_0 L_n)}$
$e^{-a/u}$
$u=\bar{v}_e$
e^{-k/k_0}
0
-2
0
2
4
6
$\left(\frac{u}{a}\right)$

Figure 3

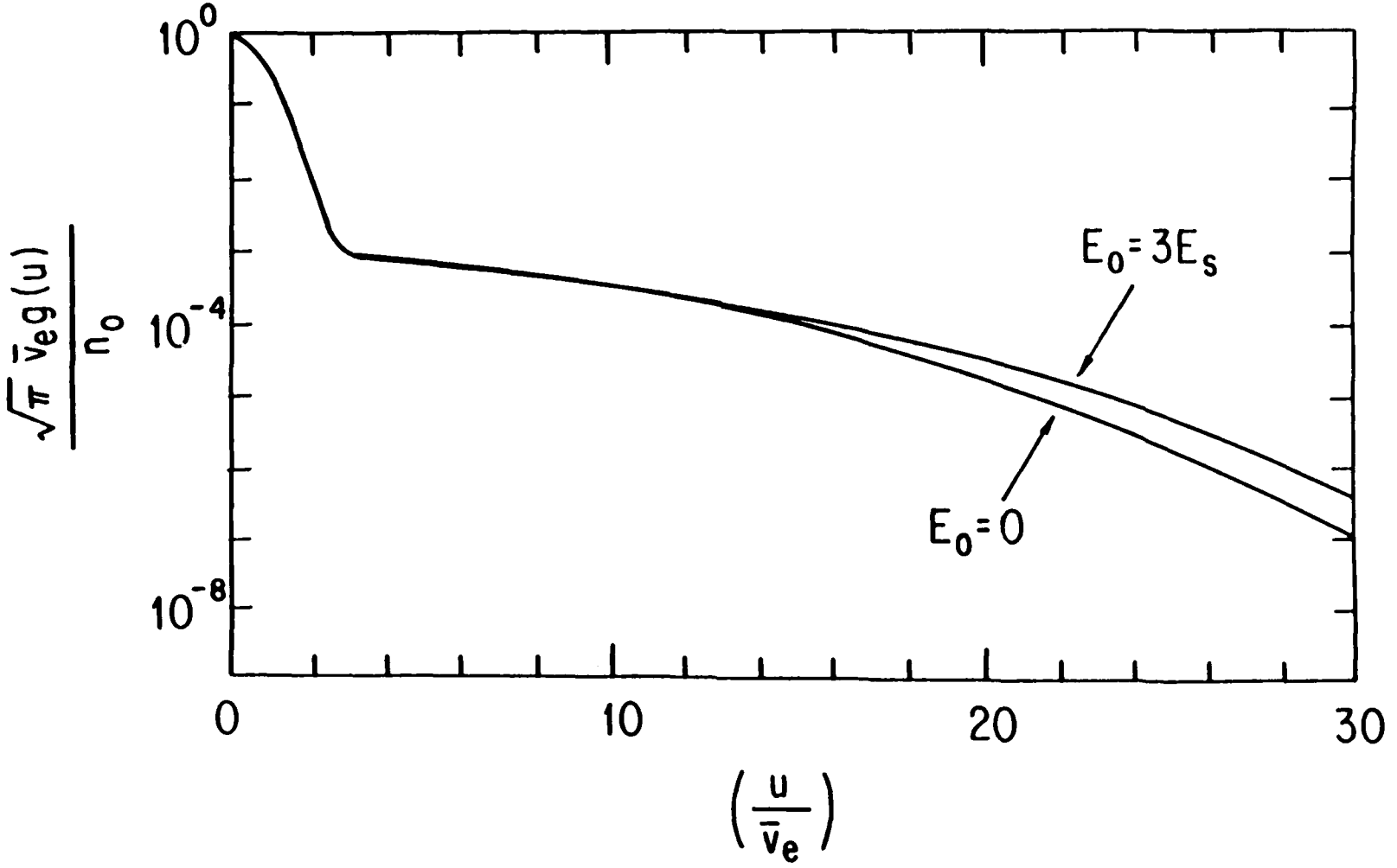
10^0
10^{-4}
10^{-8}
$\frac{\sqrt{\pi}\,\bar{v}_e g(u)}{n_o}$
$E_0 = 3E_s$
$E_0 = 0$
0
10
20
30
$\left(\frac{u}{\bar{v}_e}\right)$

Figure 4

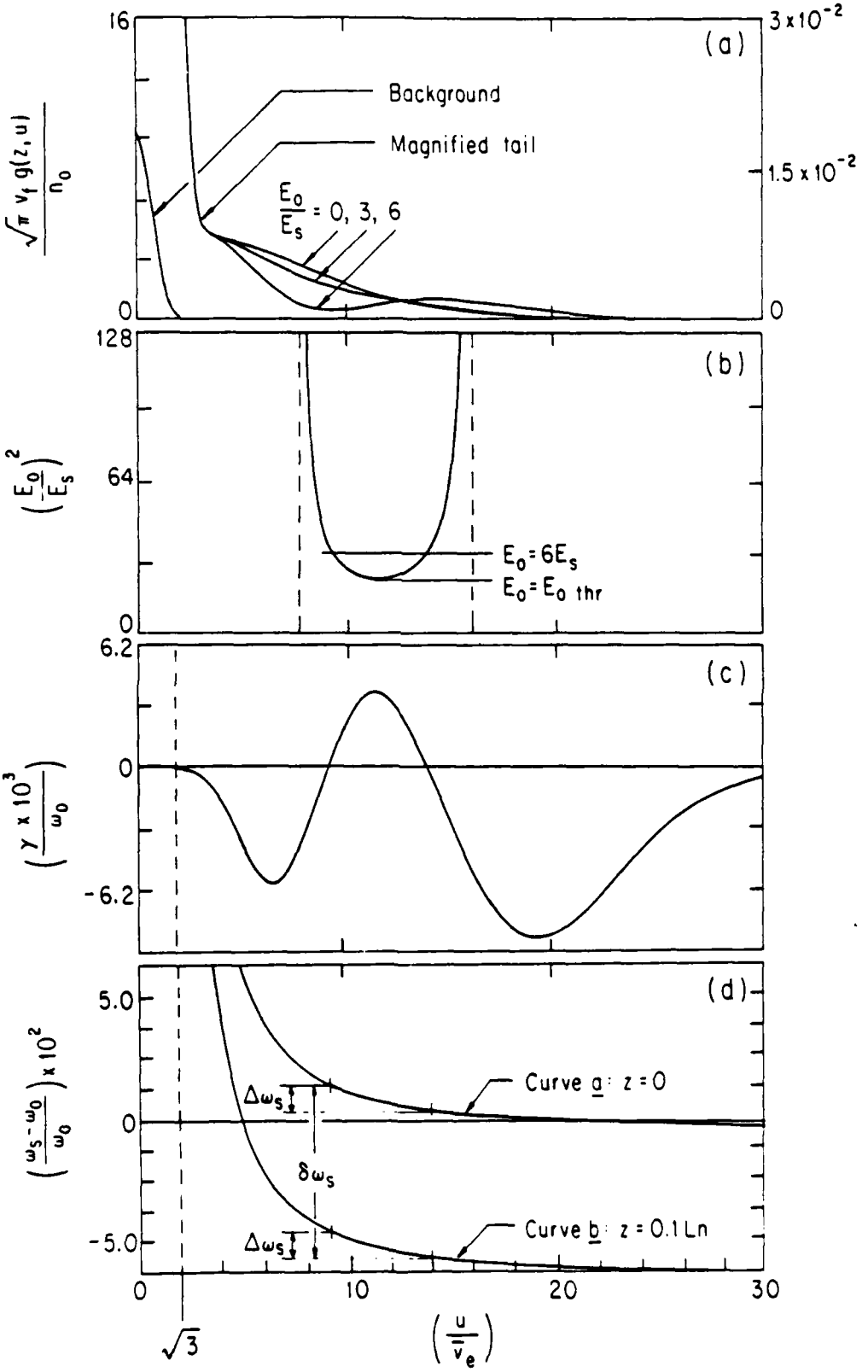
(a)
Background
Magnified tail
$\frac{E_0}{E_s}$ = 0, 3, 6
$\frac{\sqrt{\pi}\, v_f\, g(z,u)}{n_0}$
16
0
3×10^{-2}
1.5×10^{-2}
0
(b)
$\left(\frac{E_0}{E_s}\right)^2$
128
64
0
$E_0 = 6E_s$
$E_0 = E_{0\,thr}$
(c)
$\left(\frac{\gamma \times 10^3}{\omega_0}\right)$
6.2
0
-6.2
(d)
$\left(\frac{\omega_s - \omega_0}{\omega_0}\right) \times 10^2$
5.0
0
-5.0
$\Delta\omega_s$
$\delta\omega_s$
$\Delta\omega_s$
Curve a: z = 0
Curve b: z = 0.1 Ln
0
10
20
30
$\sqrt{3}$
$\left(\frac{u}{v_e}\right)$

Figure 5

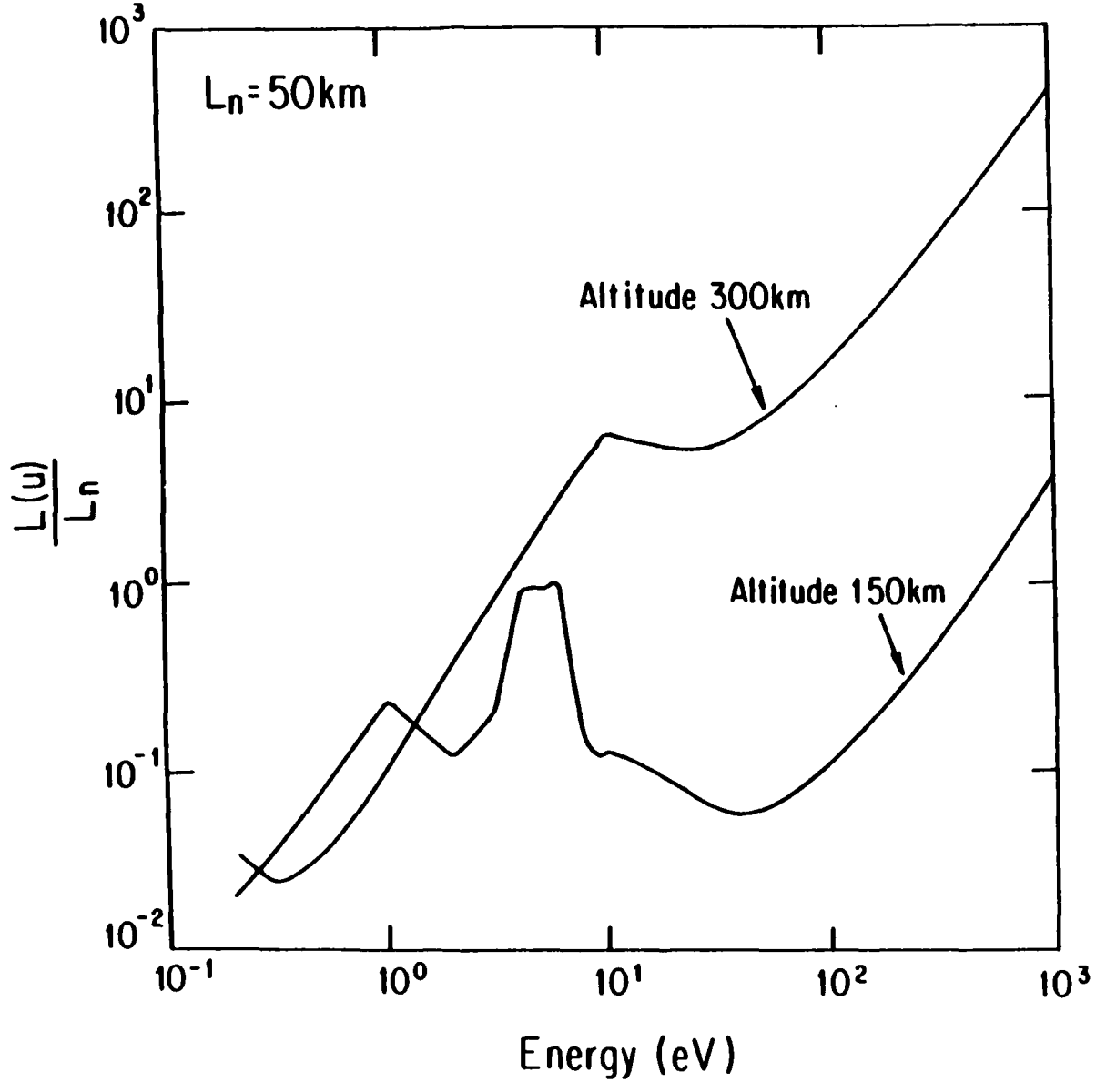
L_n=50km
Altitude 300km
Altitude 150km
$\frac{L(u)}{L_n}$
10^3
10^2
10^1
10^0
10^{-1}
10^{-2}
10^{-1}
10^0
10^1
10^2
10^3
Energy (eV)

Figure 6

TABLE 1. Electric Field and Power Densities Thresholds for Different Ionospheric Parameters*

L_n(Km)	5	10	20	50
$\nu_e(s^{-1})$	920	460	230	92
$E_{o,thr}(mV.m^{-1})$	3.27	1.64	0.82	0.33
$P_{es}(\mu W.m^{-2})$	23.6	11.8	5.89	2.36
$P_{HF}(\mu W.m^{-2})$	157	78.7	39.3	15.7

*For $a = 2\bar{\nu}_e = \nu_e L_n$, various possible combinations of ionospheric density scalelengths L_n, and bulk electron collisions ν_e yield: threshold field of (23) for sideband instability $E_{o,thr}$; threshold energy flux density in the electrostatic plasma wave P_{es}; and corresponding threshold vacuum HF power at the reflection layer P_{HF} assuming a mode conversion efficiency of $\eta = P_{es}/P_{HF} = 0.15$.

PPG-883 "Kelvin-Helmholtz Instability at the Magnetopause Boundary", C.C. Wu, August 1985.

PPG-884 "An Upwind Differencing Scheme for the Equations of Magnetohydrodynamics", M. Brio and C.C. Wu, August 1985.

PPG-885 "On the Location of Magnetopause Neutral Points", C.C. Wu, August 1985

PPG-886 "Laboratory Experiments on Magnetic Reconnection and Turbulence", R. Stenzel, W. Gekelman, and J. Urrutia, August 1985.

PPG-887 "Generation of Radial Fields in the Beat-Wave Accelerator for Gaussian Pump Profiles", R. Fedele, U. de Angeles, and T. Katsouleas, August 1985.

PPG-888 "AC Free Electron Laser", Y. T. Yan and J. M. Dawson, submitted to Phys. Rev. Lett., Sept., 1985.

PPG-889 "The Stimulated Raman Threshold I: Experiment" B. Amani and F.F. Chen, Sept. 1985.

PPG-890 "Current Drive with Fast Phase Velocity Lower Hybrid Waves", Viktor Decyk and H. Abe, September, 1985.

PPG-891 "The Subcritical-to-Supercritical Transition in Quasi-perpendicular Fast Shocks", Willis Allen Livesey, September 1985. A dissertation submitted in partial satisfaction of the requirements for the degree Doctor of Philosophy in Physics.

PPG-892 "Mode Competition in Raman Free Electron Lasers", A.T. Lin and C.-C. Lin, October 1985; submitted to Seventh International FEL Conference.

PPG-893 "The Stimulated Raman Threshold II: Theory," F. F. Chen, Sept. 1985.

PPG-894 "Theoretical Modeling of the High Temperature Helium Embritlement in Structural Alloys," J. Alhajji, October, 1985.

PPG-895 "A Review of Experimental and Theoretical Work on the Formation of Dislocation Cell Structures in Alloys," R. Amodeo and N. M. Ghoniem, October, 1985.

PPG-896 "A Data Base for Solid Breeder Blankets," R. Amadeo, S. Sharafat, and N. M. Ghoniem, October, 1985.

PPG-897 "Theory and Simulations of Broadband Electrostatic Noise in the Geomagnetic Tail," M. Ashour-Abdalla and H. Okuda, October, 1985.

PPG-898 "A Study of the Generation of Broadband Electrostatic Noise by an Ion Beam in the Magnetotail", K. Akimoto and N. Omidi, submitted to Geophys. Res. Lett., October 1985.

PPG-899 "The Effect of Magnetic Field Gradients on the Spatial Structure of ICRF Waves", Isaac R. Shokair and Robert W. Conn, submitted to Phys. Rev. Lett, Oct. 1985.

PPG-900 "U.S./JAERI Fusion Neutronics Calculational Benchmarks for Nuclear Data and Code Intercomparison," M. Youssef, J. Jung, M. Sawan, M. Nakagawa, T. Mori, K. Kosaka, to published as a joint UCLA/JAERI Report in December, 1985.

PPG-901 "A Numerical Model of Magentosphere-Ionosphere Coupling: A Preliminary Result", K. Watanabe, M. Ashour-Abdalla, T. Sato, submitted to JGR, November, 1985.

PPG-902 "On the Applications of Diffusion Theory to Neutral Atom Transport in Fusion Plasmas," M. Zhasan, R. W. Conn and G. C. Pomraning, to be submitted to Nuclear Fusion, November, 1985.

PPG-903 "Multi-Channel Far Infared Collective Scattering System for Plasma Wave Studies," D. L. Brower, H. K. Park, W. A. Peebles, N. C. Luhmann, Jr., to be submitted to Infared and Millimeter Waves, edited by K. J. Button, November, 1985.

PPG-904 "Particle Simulation of RF Heating and Current Drive", Viktor K. Decyk, presented at Third European workshop on Plasmas in the Numerical Modelling of Plasma, Varenna Italy, Sept. 10-13, 1985; November 1985.

PPG-905 "CRAY-1 Assembler and its Application to Vectorizing Particle Simulation Programs", Lingyu Xu, November, 1985.

PPG-906 "A Two-Dimensional Radial Outflow Model of Plasma at Jupiter," D.D. Barbosa, November, 1985.

PPG-907 "Mass and Energy Balance of the Cold Io Torus," M.A. Moreno and D.D. Barbosa, November, 1985.

PPG-908 "PPA Fusion Technology Status Report," M. Abdou, et al., December, 1985.

PPG-909 "Technical Issues and Requirements of Experiments and Facilities for Fusion Nuclear Technology (FINESSE Phase I Report)," M.A. Abdou et al., December, 1985.

PPG-910 "The Electrton-Cyclotron Maser Instability as the Source of Solar Type V Continuum," R.M. Winglee and G.A. Dulk, December, 1985.

PPG-911 "Computer Simulations of an Electron Beam Experiment in Space Plasma," H. Matsumoto, N. Komori, D. Donatelli and M. Ashour-Abdalla, December, 1985.

PPG-912 "Radiation Effects on the Micro Mechanical Aspects of the Fatigue Crack Initiation," Timothy D. Naughton, December, 1985.

PPG-913 "Modification of the Ionospheric Electron Velocity Distribution Function Due to Resonant Absorption of HF Waves", Merit Shoucri, G.J. Morales, and J.E. Maggs, December, 1985

END

FILMED

2-86

DTIC